Journal of the European Ceramic Society **19** (1999) 1043–1046
© 1999 Elsevier Science Limited
Printed in Great Britain. All rights reserved
PII: S0955-2219(98)00370-7
0955-2219/99/$ - see front matter

The Effect of Rare-earth (La, Sm, Dy, Ho and Er) and Mg on the Microstructure in $BaTiO_3$

Hiroshi Kishi,[a]* Noriyuki Kohzu,[a] Junichi Sugino,[b] Hitoshi Ohsato,[b]
Yoshiaki Iguchi[a] and Takashi Okuda[b]

[a]Taiyo Yuden Co., Ltd., 5607-2 Nakamuroda, Haruna-machi, Gunma 370-3347, Japan
[b]Nagaoya Institute of Technology, Gokiso-cho, Showa-ku, Nagoya 466-8555, Japan

Abstract

The effect of rare-earth elements, La, Sm, Dy, Ho and Er, on the microstructure in $BaTiO_3$(BT)–MgO–rare-earth oxide based system was studied. Larger amount of MgO was required to suppress the grain growth for the larger ionic radius rare-earth ion (La, Sm)-doped samples than for the smaller ion (Dy, Ho, Er)-doped samples. Also, substitution modes of rare-earth elements and Mg in BT lattice were investigated. The solubility of rare-earth ions in BT lattice and the substitution ratio of rare-earth ions into Ba-site decreased as ionic radius decreases. This suggests that the formation of core-shell structures in BT–MgO–rare-earth oxide based system is dependent on the substitution ratio of rare-earth ions into Ba-site.

Keywords: rare earth, microstructure-final, X-ray methods, $BaTiO_3$ and titanates, capacitors.

1 Introduction

Recently, multilayer ceramic capacitors (MLCs) with Ni electrodes have been increasingly produced to meet growing requirements for miniaturization, large capacitance and cost reduction. Saito *et al.*[1] reported that non reducible dielectrics based on $BaTiO_3$(BT)–MgO–rare–earth oxide (Ho_2O_3), developed for X7R MLCs with Ni electrodes, showed chemically heterogeneous microstructure in a grain, so-called core-shell structure. The control of microstructure has become more important to improve reliability of MLCs with very thin dielectric layer thickness less than 3 μm.

We previously reported that the microstructures and the electrical properties of BT–MgO–R_2O_3 based dielectrics were strongly affected by the kind of rare-earth oxide.[2–4] We also reported the solubility modes of rare-earth (La, Dy, Ho)-Mg into BT.[5–7] It was suggested that the microstructures and the electrical properties were influenced by the change of substitution modes of Mg and rare-earth oxide in perovskite.

The purpose of this study is to clarify the relationship between the microstructures and substitution modes of rare-earth ion in BT–MgO–rare-earth (La, Sm, Dy, Ho and Er) based system.

2 Experimental

To examine the influence of Mg and rare-earth elements on the microstructures, BT–xMgO–0·005 R_2O_3–0·015$BaSiO_3$ ($x = 0{\cdot}005$ to 0·015, R = La, Sm, Dy, Ho and Er) samples were prepared by the conventional method as follows. Hydrothermally synthesized BT with average gram size of about 0·35 μm, reagent grade MgO, fine grained rare-earth oxides (La_2O_3, Sm_2O_3, Dy_2O_3, Ho_2O_3 and Er_2O_3) and $BaSiO_3$ as a sintering aid were weighed, mixed by ball milling and then dried. The mixture added an organic binder was pressed into disks and the disks were fired m a low oxygen atmosphere after the binder was burned out. The microstructure of the samples was observed by scanning electron microscopy (SEM). The ceramics was crushed and ground into powder, and then the phase transition of the samples was characterized by differential scanning calorimetry (DSC).

In order to analyze solubility modes of rare-earth elements and Mg in BT, another samples were also prepared according to following formulae, $(Ba_{1-2x}R_{2x})Ti_{1-x}Mg_{x})O_3$: (Ba-site: rare-earth Ti-site: Mg replacement model) ($x = 0{\sim}0{\cdot}15$). The raw materials,

---

*To whom correspondence should be addressed. Fax: +81-027-360-8307; e-mail: hkishi@jty.yuden.co.jp

$BaCO_3$, $MgCO_3$, TiO_2, La_2O_3, Sm_2O_3, Dy_2O_3, Ho_2O_3 and Er_2O_3 were mixed and then calcined at 1250°C. Identification of precipitated phases was performed by powder XRD analysis. The solubility mode was monitored by the behavior of the lattice parameters as a function of the doping amount x. In order to avoid the influence on the lattice parameters by crystal structure change according to compositions, high-temperature powder XRD analysis was also earned out at higher temperature (300°C) than the Curie point. The lattice parameters were determined precisely using the whole-powder-pattern decomposition method (WPPD[8]) program as described the previous paper.[9]

3 Results and Discussion

3.1 Microstructure

Figure 1 shows effect of MgO content on the mean grain size for the surface of the various rare-earth doped samples sintered at 1320°C. The mean grain size was determined by the intercept method using SEM micrograph. The mean grain size decreased with increasing MgO content. Particulary, grain growth occurred in the La- and Sm-doped samples with 0·5 mol% MgO. The microstructure for the La- and Sm-doped samples strongly depended on MgO content. On the other hand, they were almost independent on MgO content for the Dy-, Ho- and Er-doped samples. Figure 2 shows the effect of MgO content on the DSC peak temperature for the samples sintered at 1320°C. Since a core is composed of pure BT, the temperature of DSC peak for the samples having core-shell structures should be the Curie temperature of BT. The peak temperature was unchanged practically for the Dy-, Ho- and Er-doped samples. However, in case of the La- and Sm-doped samples with 0·5 mol% MgO, the peak temperature shifted down to around 100°C.

From these results, it was found that a larger amount of MgO was necessary to form the core-shell structure for the La- and Sm-doped samples than for the Dy-, Ho- and Er-doped samples. It seemed that the higher diffusivity into the core phase of La and Sm ions compared with Dy, Ho and Er ions is related to their ionic radii.

3.2 Solubility mode

The ionic radii of Ba, Ti, La, Sm, Dy, Ho, Er and Mg are summarized as follows. Ba-site (12 coordinate): $Ba^{2+} = 1{\cdot}61$ Å, $La^{3+} = 1{\cdot}36$ Å, $Sm^{3+} = 1{\cdot}24$ Å, $Dy^{3+} = 1{\cdot}253$ Å, $Ho^{3+} = 1{\cdot}234$ Å, $Er^{3+} = 1{\cdot}234$ Å; Ti-site (6 coordinate): $Ti^{4+} = 0{\cdot}605$ Å, $La^{3+} = 1{\cdot}032$ Å, $Sm^{3+} = 0{\cdot}958$ Å, $Dy^{3+} = 0{\cdot}912$ Å, $Ho^{3+} = 0{\cdot}901$ Å, $Er^{3+} = 0{\cdot}89$ Å, $Mg^{2+} = 0{\cdot}72$ Å. The ionic radii of Dy, Ho and Er ions in 12 coordinate are based on the relationship between coordination number and effective ionic radii after Shannon's table.[10] The ionic radii of rare-earth elements locate just intermediate of those of Ba and Ti. Therefore, rare-earth elements are considered to dissolve in both Ba- and Ti-sites.[11,12] On the other hand, the radius of Mg ion is close to that of Ti ion. Mg is considered to dissolve in the Ti-site.[11] In the previous study,[5] we confirmed that Mg reacts with BT at low temperatures compared with Ho and dissolves into Ti-site. Therefore, taking the compensation of electrical charge into consideration, we synthesized the samples according to the following compositions: $(Ba_{1\text{-}2x}R_{2x})(Ti_{1\text{-}x}Mg_x)O_3$.

Table 1 shows the precipitated phases of the samples. It was found that single phase of BT solid solution was obtained in wide range for larger rare-earth ion (La, Sm) substituted samples compared with smaller rare-earth ion (Dy, Ho, Er) substituted samples. No secondary phase appeared in the range up to $x = 0{\cdot}150$ for the La–Mg substituted samples. On the other hand, in case of the smaller rare-earth ion (Dy, Ho, Er) and Mg substituted samples, the

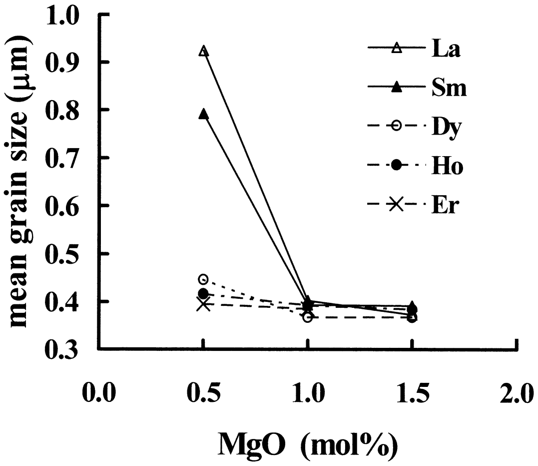

Fig. 1. Effect of MgO content on the mean grain size for the various rare-earth doped samples.

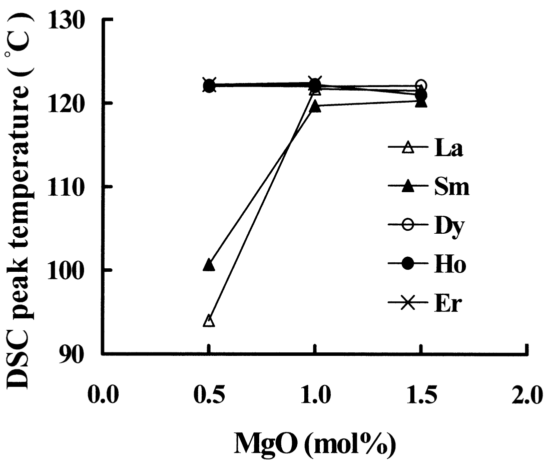

Fig. 2. Effect of MgO content on DSC peak temperature for the various rare-earth doped samples.

Table 1. Precipitated phases of the samples calcined at 1250°C

x	*La–Mg system*	*Sm–Mg system*	*Dy–Mg system*	*Ho–Mg system*	*Er–Mg system*
0·002	BT(T)	BT(T)	BT(T)	BT(T)	BT(T)
0·005	BT(T)	BT(T)	BT(T)	BT(T)	BT(T)
0·010	BT(T)	BT(T)	BT(T) + *R*T2	BT(T) + *R*T2	BT(T) + *R*T2
0·015	BT(C)	BT(T)	BT(T) + *R*T2	BT(T) + *R*T2	BT(T) + *R*T2
0·020	BT(C)	BT(T)	BT(T) + *R*T2	BT(C) + *R*T2	BT(C) + *R*T2
0·030	BT(C)	BT(C)	BT(C) + *R*T2	BT(C) + RT2	BT(C) + *R*T2 + *R*
0·050	BT(C)	BT(C)	BT(C) + *R*T2 + *R*	BT(C) + *R*T2 + *R*	BT(C) + *R*T2 + *R* + *R*MT
0·100	BT(C)	BT(C) + *R*T + *R*T2	BT(C) + *R*T2 + *R* + *R*MT	BT(C) + *R*T2 + *R* + *R*MT	—
0·150	BT(C)	—	BT(C) + *R*T2 + *R* + *R*MT	BT(C) + *R*T2 + *R* + *R*MT	—

BT(T), BaTiO$_3$ (tetragonal); BT(C), BaTiO$_3$ (cubic); *R*T, R_2TiO$_5$; *R*T2, R_2Ti$_2$O$_7$; *R*, R_2O$_3$; *R*MT, R_2MgTiO$_6$.

single phase of BT solid solution was only obtained up to $x = 0{\cdot}005$. As secondary phases, pyrochlore (R_2Ti$_2$O$_7$), R_2O$_3$, R_2MgTiO$_6$, etc., were observed. The crystal structure of BT solid solutions changed from tetragonal to cubic at $x = 0{\cdot}015$ for the La–Mg substituted sample, $x = 0{\cdot}020$ for the Ho–Mg and Er–Mg substituted samples, and $x = 0{\cdot}030$ for the Sm–Mg and Dy–Mg substituted samples, respectively.

Figure 3 shows the lattice parameters of the samples at 300°C, as determined by WPPD. It appeared that the solubility behavior between the larger rare-earth ion (La, Sm) substituted samples and the smaller rare-earth ion (Dy, Ho, Er) substituted samples was clearly different. In case of the La–Mg and Sm–Mg substituted samples, the lattice parameter decreased monotonously as a function of x. The changes of the lattice parameters for the both samples are divided into two stages. The lattice parameter decreased gradually up to $x = 0{\cdot}050$ for the La–Mg substituted sample, $x = 0{\cdot}030$ for the Sm–Mg substituted sample in the first stage, and then they decreased steeply in the second stage. On the other hand, in the case of the Dy–Mg, Ho–Mg and Er–Mg substituted samples, both the decrease and the increase in the lattice parameters were observed. The change of the lattice parameter on these samples showed similar behavior as follows. Firstly, the lattice parameter decreased gradually up to $x = 0{\cdot}050$ for the Dy–Mg substituted sample, $x = 0{\cdot}010$ for the Ho–Mg substituted sample and $x = 0{\cdot}005$ for the Er–Mg substituted sample. In the second stage, they showed no change up to $x = 0{\cdot}100$ for the Dy–Mg substituted sample, $x = 0{\cdot}025$ for the Ho–Mg substituted sample and $x = 0{\cdot}010$ for the Er–Mg substituted samples. In the third stage, the increase of the lattice parameter observed up to $x = 0{\cdot}150$ for the Dy–Mg substituted sample, $x = 0{\cdot}100$ for the Ho–Mg substituted sample and $x = 0{\cdot}030$ for the Er–Mg substituted sample. It was found that the increase of the lattice parameter occurred at lower substitution content as rare-earth ionic radius decreases. In case of the Ho–Mg and Er–Mg substituted samples, the lattice parameter showed little change above $x = 0{\cdot}100$ for the Ho–Mg substituted sample and $x = 0{\cdot}030$ for the Er–Mg substituted sample. It is considered that the solubility of rare-earth ions into BT lattice decreased as ionic radius decreases.

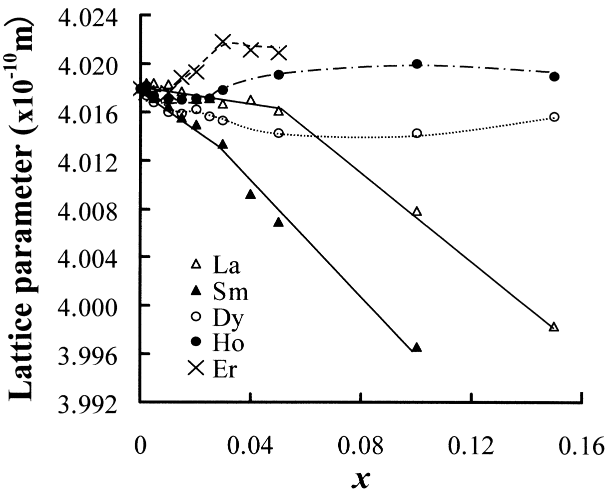

Fig. 3. Lattice parameters of (Ba$_{1\text{-}2x}R_{2x}$)(Ti$_{1\text{-}x}$Mg$_x$)O$_3$(R = La, Sm, Dy, Ho and Er) solid solutions measured at 300°C as a function of x.

These phenomena can be explained by the different substitution modes of rare-earth elements at cation sites. The increase in lattice parameter is based on Ti-site replacement by larger cation (Mg, rare-earth) than Ti ion. The decrease in lattice parameter is based on Ba-site replacement by smaller cation (rare-earth) than Ba ion. In case of the La–Mg and Sm–Mg substituted samples, the change of the lattice parameter is considered as follows. La and Sm ions mainly substitute for Ba-site accompanied with Ti-site substitution of Mg ions. The difference of the gradient between the first stage and the second stage depends on the substitution ratio of Mg ions into Ti-site. The substitution ratio of Mg ions into Ti-site in the first stage is larger than that in the second stage.

On the other hand, the change of the lattice parameter on the smaller rare-earth (Dy, Ho, Er) and Mg substituted samples is considered as follows. In the first stage, rare-earth (Dy, Ho, Er) mainly substitute in Ba-site accompanied with Ti-site substitution of Mg ions. The substitution ratio of rare-earth (Dy, Ho, Er) into Ba-site decreased in the second stage and then rare-earth ions mainly dissolve in Ti-site in the third stage.

It appeared that the substitution ratio of rare-earth ions into Ba-site decreased as ionic radius decreases. This can be attributed to decrease of radius difference between rare-earth and Ti ion. It also appeared that the solubility of rare-earth ions in BT lattice strongly depended on its ionic radius. Therefore, it is considered that the formation of core-shell structures in the BT–MgO–R_2O_3 based system is dependent on the substitution ratio of rare-earth ions into Ba-site. The present results suggest that the larger ionic radius rare-earth ions behave more likely as donor dopants than the smaller ionic radius rare-earth ions. Thus further investigation of the solubility modes of rare-earth ions in the shell phase is necessary to improve reliability of MLCs with nickel electrodes.

4 Conclusion

The effect of various rare-earth addition on the microstructure in BT–MgO–rare-earth oxide based system was confirmed. Larger amount of MgO was necessary to suppress the grain growth and form the core-shell structure for the larger ion (La, Sm)-doped samples than for the smaller ion (Dy, Ho, Er)-doped samples.

The solubility modes of rare-earth elements and Mg into BT lattice were also investigated by high-temperature powder XRD. The lattice parameters of various rare-earth and Mg substituted samples were determined at higher temperature than Curie point. The solubility of rare-earth ions in BT lattice decreased as ionic radius decreases. It was confirmed that the larger ion, La and Sm, mainly dissolved Ba-site, and the smaller ion, Dy, Ho and Er, dissolved both Ba- and Ti-sites. The substitution ratio of rare-earth into Ba-site in BT lattice decreased as ionic radius decreases. This suggests that the formation of the core-shell structures in BT–MgO–rare-earth oxide based system is dependent on the substitution ratio of rare-earth ions into Ba-site.

References

1. Saito, H., Chazono, H., Kishi, H. and Yamaoka, N., X7R multilayer ceramic capacitors with nickel electrodes. *Jpn. J. Appl. Phys.*, 1991, **30**, 2307.
2. Okino, Y., Shizuno, H., Kusumi, S. and Kishi, H., Dielectric properties of rare-earth-oxide-doped $BaTiO_3$ ceramics fired in reducing atmosphere. *Jpn. J. Appl. Phys.*, 1994, **33**, 5393.
3. Okino, Y., Kohzu, N., Mizuno, Y., Honda, M., Chazono, H. and Kishi, H., Effects of the microstructure on dielectric properties for $BaTiO_3$-based MLC with Ni electrode. *Key Engineering Materials*, 1999, **157–158**, 9.
4. Kishi, H., Chazono, H., Kohzu, N., Okino, Y., Honda, M. and Mizuno, Y., Microstructure and electrical properties of rare-earth oxide and MgO doped $BaTiO_3$ fired in reducing atmosphere. In *Proceedings of 9th CIMTEC. World Ceramic Congress and Forum on New Materials (Florence, Italy, 14–19 June, 1988)*, in press.
5. Kishi, H., Okino, Y., Honda, M., Iguchi, Y., Imaeda, M., Takahashi, Y., Ohsato, H. and Okuda, T., The effect of MgO and rare-earth oxide on formation behavior of core-shell structure in $BaTiO_3$. *Jpn. J. Appl. Phys.*, 1997, **36**, 5954.
6. Watanabe, K., Ohsato, H., Kishi, H., Okino, Y., Kohzu, N., Iguchi, Y. and Okuda, T., Solubility of La–Mg and La–Al in $BaTiO_3$. *Solid State Ionics*, 1998, **108**, 129.
7. Kishi, H., Kohzu, N., Okino, Y., Takahashi, Y., Ohsato, H., Watanabe, K., Sugino, J. and Okuda, T., Effect of rare-earth oxides on formation of core-shell structures in $BaTiO_3$. In *Proceedings of International Symposium on Dielectric Ceramics (Cincinnati, OH, USA, 2–6 May, 1998), Am. Ceram. Soc.*, in press.
8. Toraya, H., Whole-powder-pattern fitting without reference to A structual model application to X-ray powder diffraction data. *J. Appl. Crystallogr.*, 1986, **16**, 440.
9. Ohsato, H., Imaeda, M., Okino, Y., Kishi, H. and Okuda, T., Lattice parameters of $BaTiO_3$ solid solutions containing Dy and Ho at high temperature. *Advances in X-ray Analysis*, 1997, **40** (CD-ROM: International Centre for Diffraction Data).
10. Shannon, R. D., Revised effective ionic radii and systematic studies of interatomic distance in halides and chalcogenides. *Acta. Crystallogr.*, 1976, **A32**, 751.
11. Lewis, G. V. and Catlow, C. R. A., Defect studies of doped and undoped barium titanate using computer simulation techniques. *J. Phys. Chem. Solids*, 1986, **47**, 89.
12. Takada, K., Chang, E. and Smith, D. M., *Rare Earth Additions to $BaTiO_3$*. Advances in Ceramics, Vol. 19, Multilayer Ceramic Devices, eds. J. B. Blum and W. R. Cannon. *Am. Ceram. Soc.*, Westerville, OH, 1987, pp. 147–151.